Senior Thesis

The Effect of the Bragg Angle on the Electrostatic Potential of Silicon

by
Matt Karrer
1990

Submitted as partial fulfillment of the requirments for the degree of Bachelor of Science in Geology and Mineralogy at The Ohio State University, Spring Quarter, 1990

Approved by:

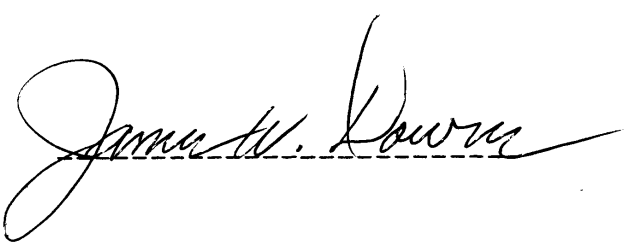

Introduction

The electrostatic potential of a crystal shows the work needed to move a positive charge to any point in the lattice from infinity. The electrostatic potential is a quantum mechanically observable property and as such gives a more realistic picture of charge distribution than does the ambiguous notions of atomic charge in a crystal (Politzer and Truhlar 1987). Furthermore, atomic radii obtained from the electrostatic potential are at odds with the classical picture of small cations and large anions (Downs and Gibbs 1987). Since the electrostatic potential shows the work needed to introduce a point charge from infinity, it has been used to study protonation processes (Downs 1989). Not only does the electrostatic potential give clues as to where a positive charge will be attracted, it also gives insight into the probable path of the point charge (Politzer and Truhlar 1981). Another area of promise for the electrostatic potential is its relationship to energetics of a system via density functional theories (Politzer and Truhlar 1981). Since the electrostatic potential is derived from experimental diffraction data, the extent to which experimental parameters effect the electrostatic potential is of interest. The Bragg angle is one of those parameters and its effect on the electrostatic potential of crystalline silicon will be the focus of this paper.

Methods

X-ray structure factors are Fourier components of the thermal average charge density in a crystallographic unit cell and as such they can be used to determine physical properties that depend on electron density (Stewart 1979). One such property is the electrostatic potential. The electrostatic potential is the first inner moment of the electron density (Stewart 1979) and is given by:

$$\phi(\underset{\sim}{r}) = Z_a\ |\underset{\sim}{R}_a - \underset{\sim}{r}|^{-1} - \int \rho(\underset{\sim}{r})\ |\underset{\sim}{r}' - \underset{\sim}{r}|^{-1}\ d\underset{\sim}{r} \qquad (1)$$

Here Z_a is the charge on the nucleus of some atom, a. R_a is its nuclear coordinate and p(r) is the electron density. The first term of the equation for the electrostatic potential includes contributions from the nucleus while the second term includes contributions from the electron distribution. The electrostatic potential is simply the total electric potential at any given point due to the total unperturbed charge distribution. The Fourier sum of equation (1) is:

$$\phi(\underset{\sim}{r}) = (4\pi V)^{-1} \Sigma F_H \exp(-2\pi i H \cdot \underset{\sim}{r})\ (\sin\Theta / \lambda)^{-2} \qquad (2)$$

where V is the unit cell volume, F_H is the experimentally derived structure factor, H is the Bragg vector, Θ, is the Bragg angle, and λ, is the wavelength. This form of the equation for the electrostatic potential allows derivation of the electrostatic potential from experimentally derived structure factors (Stewart 1979).

Obtaining the electrostatic potential from X-ray

structure factors is not as simple as simply solving equation (2) however. The term $(\sin\Theta/\lambda)$ poses grave problems when the Bragg angle is zero in the F(000) term. To circumvent this problem a combination of Fourier-series and direct space lattice summations are used such that:

$$\phi(\underset{\sim}{r}) = \Delta\phi(\underset{\sim}{r}) + \phi(\underset{\sim}{r})_{IAM} + \phi_0 \qquad (3)$$

where $\Delta\phi(\underset{\sim}{r})$ is the deformation electrostatic potential and is the difference between the thermal mean electrostatic potential as observed from experimental data and the electrostatic potential derived from a model (Potitzer and Truhlar 1981). The second term in the equation $\phi(\underset{\sim}{r})_{IAM}$, is the model electrostatic potential which is added back by direct space lattice summation. Finally, ϕ_0 , is a constant added that insures that the integral of the electrostatic potential over the crystal is zero which is necessary for a neutral crystal. (Stewart 1979)

The model usually chosen in such cases is the Independent Atom Model or IAM. In this model, the spherically averaged charge density is used, and is calculated from Hartree-Fock wave functions (Politzer and Truhlar 1981). The model is then superposed onto mean nuclear positions arrived at from the X-ray experiment (Stewart 1979).

The equation for the deformation potential is similar to equation (2) and is given by the Fourier series:

$$\Delta\phi(\underset{\sim}{r}) = (4\pi V)^{-1} \Sigma\Delta F_H \exp(-2\pi i \underset{\sim}{H}\cdot\underset{\sim}{r}) (\sin\Theta/\lambda)^{-2} \qquad (4)$$

where $\Delta F_H = F_O - F_{IAM}$ and is the difference between

experimentally derived structure factors and structure factors obtained using the Independent Atom Model (Stewart 1979).

At a sufficient distance (about 1 A.) from the nucleus the experimental observed electrostatic potential and the deformation potential are very similar. Furthermore, near the nucleus, the electrostatic potential shows only the very large peaks associated with the nucleus. Because of this, the electrostatic potential is of interest in extranuclear regions. This allows the reintroduction of the static spherically averaged model with direct space methods. The result is an approximate representation of the total electrostatic potential of the unit cell of a crystal. (Stewart 1979)

As can be seen in both the equation for the electrostatic potential and deformation potential, $\sin\theta/\lambda$ occurs as an inverse squared term in the summation. Since lambda is fixed by experimental conditions, we need only examine $\sin\theta$. As the Bragg angle increases, each successive term in the summation decreases. The net effect this has on the electrostatic potential is that higher angle reflections are not as important as low angle reflections for an accurate representation of the electrostatic potential.

Results

Crystalline silicon has a diamond structure type with space group Fd3m and a lattice constant of 5.4310 A. Eighteen reflections were used in calculating the

electrostatic potential. The data represents an accurate set up to a maximum $(\sin\theta/\lambda)$ = 1.05 A^{-1}. (Spackman 1986)

Electrostatic potential maps were completed using the Valray system (Stewart and Spackman 1983).

A map of the total electrostatic potential is given in Fig.1. The map is the electrostatic potential at $\sin\theta/\lambda$=1.04 A^{-1} which includes all reflections in the data set. Negative contours are dashed, positive contours are solid, and the zero contour is represented as a large dashes. Positive contours near nuclear positions are omitted. Silicon atoms in the map show up quite clearly in the map and their nuclei are shown by plus signs. The plus signs at the edge of the maps are nuclei positions that are either above or below the mapped plane. The mapped plane is the [110] plane with a horizontal dimension of 5.76 A. and a vertical dimension of 4.07 A. Local maxima occur at each of the nuclei in the plane and minima exist removed from bonded silicons. Minimum values in the map for the electrostatic potential of silicon are on the order of -.770 e/A, and values in the saddle between bonded silicon are typically -.098 e/A.

Figure 2 shows the deformation potential. The mapped plane is the same as that in Fig. 1 as is the value for sin θ/λ. The deformation potential represents the difference between the observed electrostatic potential and a static model potential. Electronegative regions in the deformation potential maps show where there is a concentration of electron density relative to Independent Atom Model (Stewart

1979). The nuclei have a potential near -.04 e/A and regions in the bond area between silicon atoms have a negative potential near -.1 e/A. Bonding between silicon atoms localizes charge distribution in the bonded region which shows itself as the large negative wells in the deformation potential map.

As $\sin\theta/\lambda$ is decreased reflections used in the computation of the electrostatic potential are limited. Fig.3 shows the electrostatic potential calculated at two points for varying values of $\sin\theta/\lambda$. The point (.25,0,.25) lies on the saddle between bonded silicon while (.125,.125,.309) is a point slightly removed from the silicon nucleus along Z. From the graph it is apparent that when $\sin\theta/\lambda$ is below .4 A^{-1} values of the electrostatic potential begin to fluctuate. This value represents an electrostatic potential where only six unique reflections were used in computation and suggest a minimum level of resolution necessary for obtaining accurate potential maps of silicon.

Maximum and minimum values of the deformation density are plotted against $\sin\theta/\lambda$ in Fig.4. Once again, below a value of $\sin\theta/\lambda$ =.4 A^{-1} fluctuation in the electrostatic potential occurs.

Comparison of deformation potential maps for different values of $\sin\theta/\lambda$ is shown in Fig. 5. The left hand portion of the map shows the electrostatic potential at $\sin\theta/\lambda$ =1.04 A^{-1} while the right hand side is for a value of .37 A^{-1} which includes only 5 unique reflections. The major differences

are that as less reflections are used in the computation of the deformation density the values for the deformation potential at nuclear positions changes markedly. The left side of Fig. 5 shows a deformation potential value of -.039 e/A at the nucleus while the right shows a value of -.012 e/A. The deformation potential values change in binding regions as well, but not as dramatically, with the left side showing a value of -.098 e/A and the right side showing -.086 e/A. This indicates that high angle data is more important for retrieving the electrostatic potential at nuclei positions than it is for extra nuclear regions.

Conclusions

The Bragg angle plays an important role in the general features of the electrostatic potential for silicon. As high angle data is limited, the magnitude of the electrostatic potential at any given point fluctuates. The onset of this fluctuation in silicon begins at a maximum $\sin\theta/\lambda$ value near .4 A^{-1} where the magnitude of potential maps are similar to those computed with the full data set. Similar results occur in mapping the deformation potential for silicon. With a decrease in $\sin\theta/\lambda$ potential accumulation due to the experimental potential in the binding regions decreases a small amount relative to that of the Independent Atom Model while the deformation potential at nuclear positions shows a large decrease in magnitude. These results suggest that a data set with a maximum $\sin\theta/\lambda > .4$ A^{-1} is necessary for an accurate determination of the electrostatic potential of

silicon.

References

Clementi, E. and Roetti, C. (1974) Roothaan-Hartree-Fock wave functions: Basis functions and their coefficients for ground and certain excited states of neutral and ionized atoms, Z < 54. Atomic Data and Nuclear Data Tables, 14, 177-478.

Downs, J.W. (1989) Possible sites for protonation in B-Mg_2SiO_4 from an experimentally derive electrostatic potential. American Mineralogist, 74, 1124-1129.

Downs, J.W., Gibbs, G.V. (1987) An exploratory examination of the electron density an electrostatic potential of phenakite. American Mineralogist, 72, 769-777.

Politzer, P., and Truhlar, D.G. (1981) Introduction: The role of the electrostatic potential in chemistry. In P. Politzer and D.G. Truhlar, Eds., Chemical applications of atomic and molecular electrostatic potentials, p. 1-6. Plenum Press, New York.

Spackman, M.A. (1986) The electron Distribution in silicon. A Comparison between experiment and theory. Acta Crystallographica, A42, 271-281.

Spackman, M.A. and Hill, R.J.,Gibbs, G.V. (1987) Exploration of structure and bonding in stishovite with Fourier and psuedoatom refinement methods using single crystal and powder x-ray diffraction data. Physics and Chemistry of Minerals, 14, 139-150.

Spackman, M.A., and Stewart, R.F. (1981) Electrostatic potentials in crystals. In P.Politzer and D.G. Truhlar, Eds., Chemical applications of atomic and molecular electrostatic potentials, p. 407-425. Plenum Press, New York.

Stewart, R.F. (1979) On the mapping of Electrostatic properties from Bragg Diffraction Data. Chemical Physical Letters, 65, 335-342

Stewart, R.F. and Spackman, M.A. (1983) VALRAY Users Manual. Department of Chemistry, Carnegie-Mellon University, Pittsburgh, Pennsylvania.

Explanation of Figures

Fig. 1 The electrostatic potential of silicon, $(\sin\theta/\lambda)=1.04\ A^{-1}$. The map is in the [110] plane with a horizontal axis of 5.75985 A parallel to [110] and vertical axis of 4.07283 A parallel to Z. Contour interval is 0.1 e/A with negative and zero contours dashed. Nuclear positions are marked with a +.

Fig. 2 The deformation potential of silicon. Plane is as Fig.1. Contour interval is 0.01 e/A.

Fig. 3 Graph of the electrostatic potential of silicon at two points vs. $(\sin\theta/\lambda)$. Data points represent reflections used. The lower curve represents a point located in the saddle between bonded silicon atoms while the upper curve is for a point slightly removed from the nucleus along Z.

Fig. 4 Maximum and minimum values of the deformation potential plotted against values of $(\sin\theta/\lambda)$. These are the local extremes for the map as in Fig. 2.

Fig. 5 Deformation potential of silicon at $(\sin\theta/\lambda)=1.04\ A^{-1}$ (left hand side) and $(\sin\theta/\lambda)=.3683\ A^{-1}$ (Right hand side). Mapped plane as in Fig. 1. Contour interval 0.01 e/A.

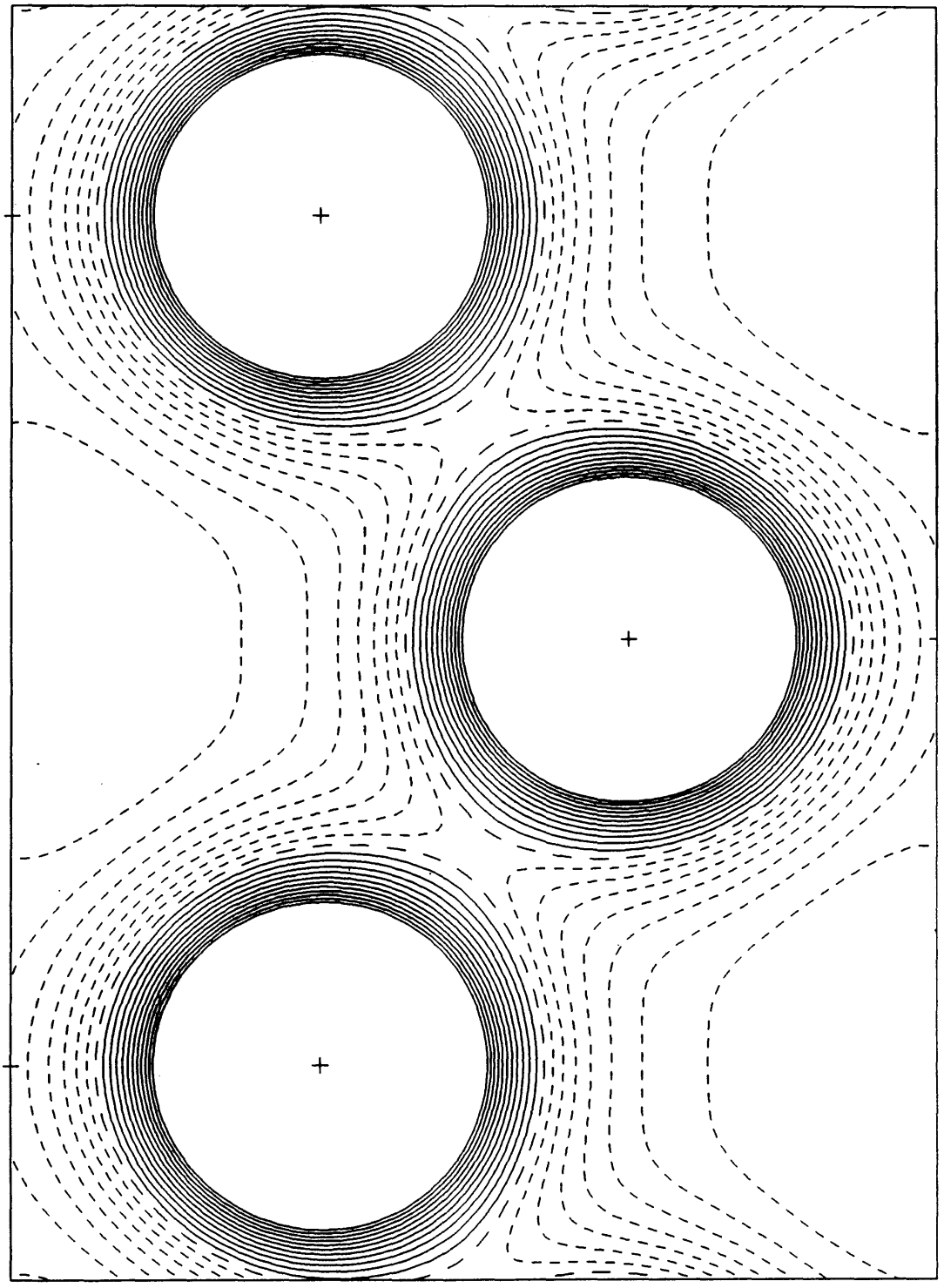

Fig. 1

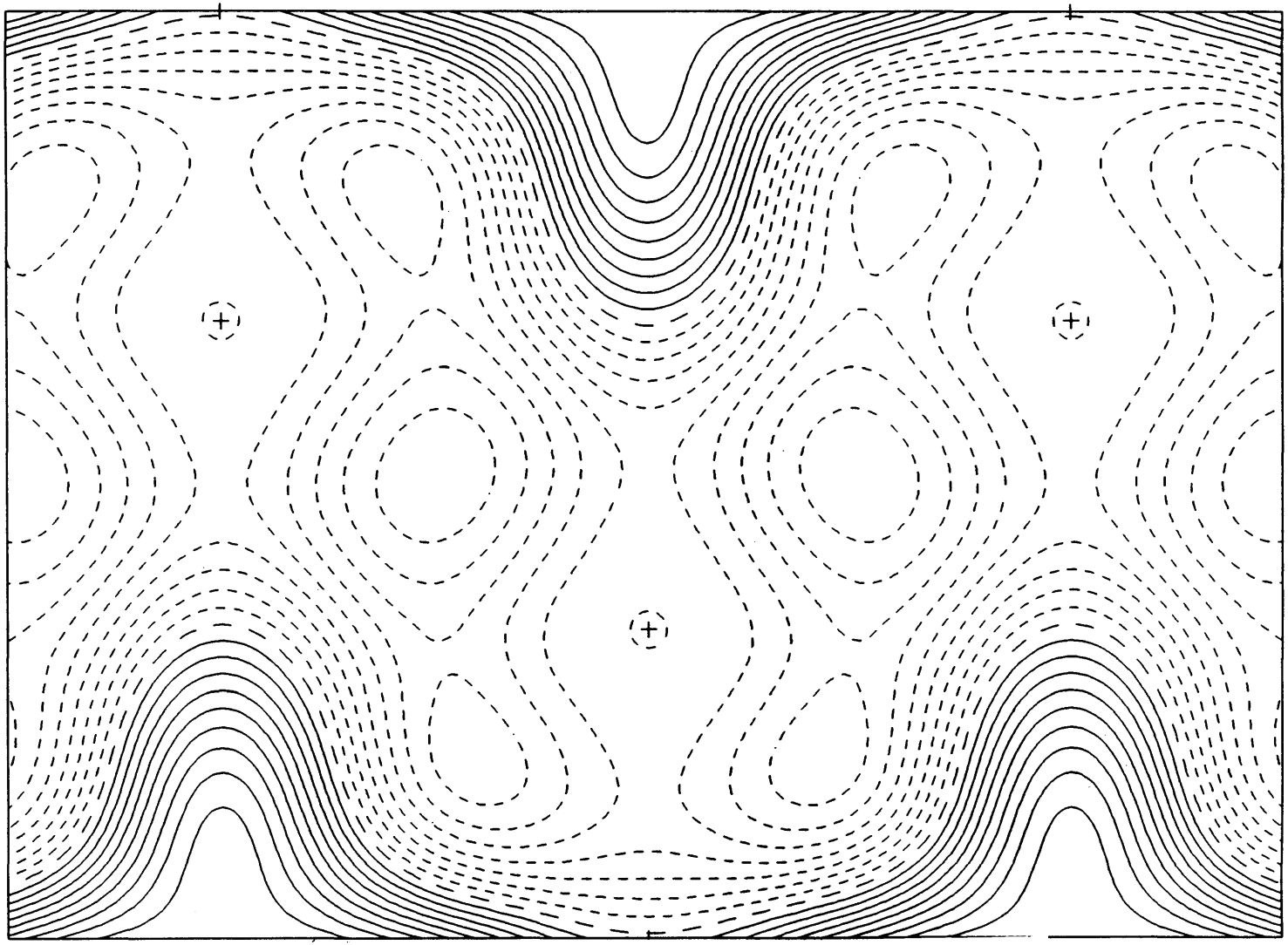

Fig. 2

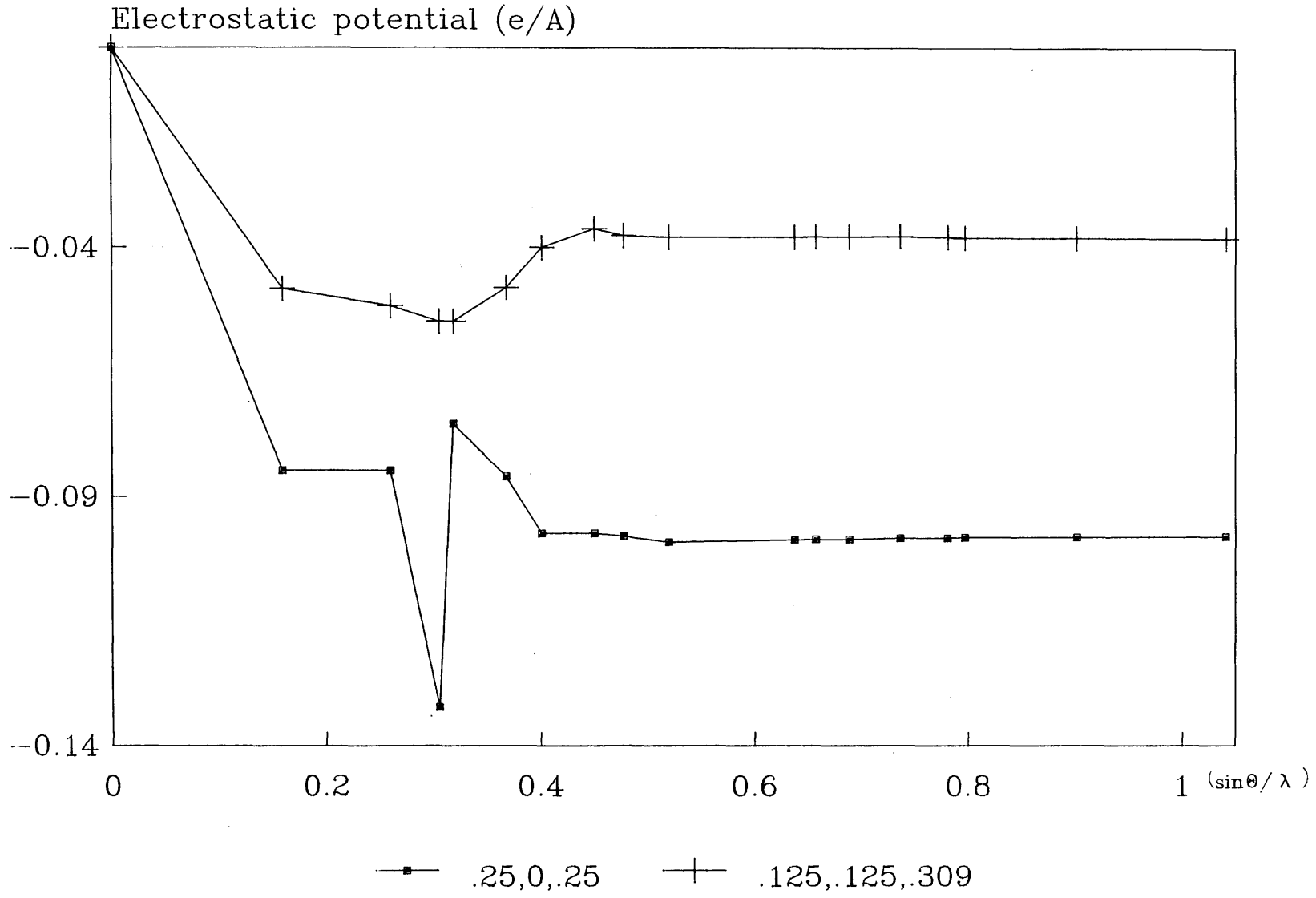
Electrostatic potential (e/A)
-0.04
-0.09
-0.14
0
0.2
0.4
0.6
0.8
1
(sinΘ/λ)
.25,0,.25
.125,.125,.309

FIG.3

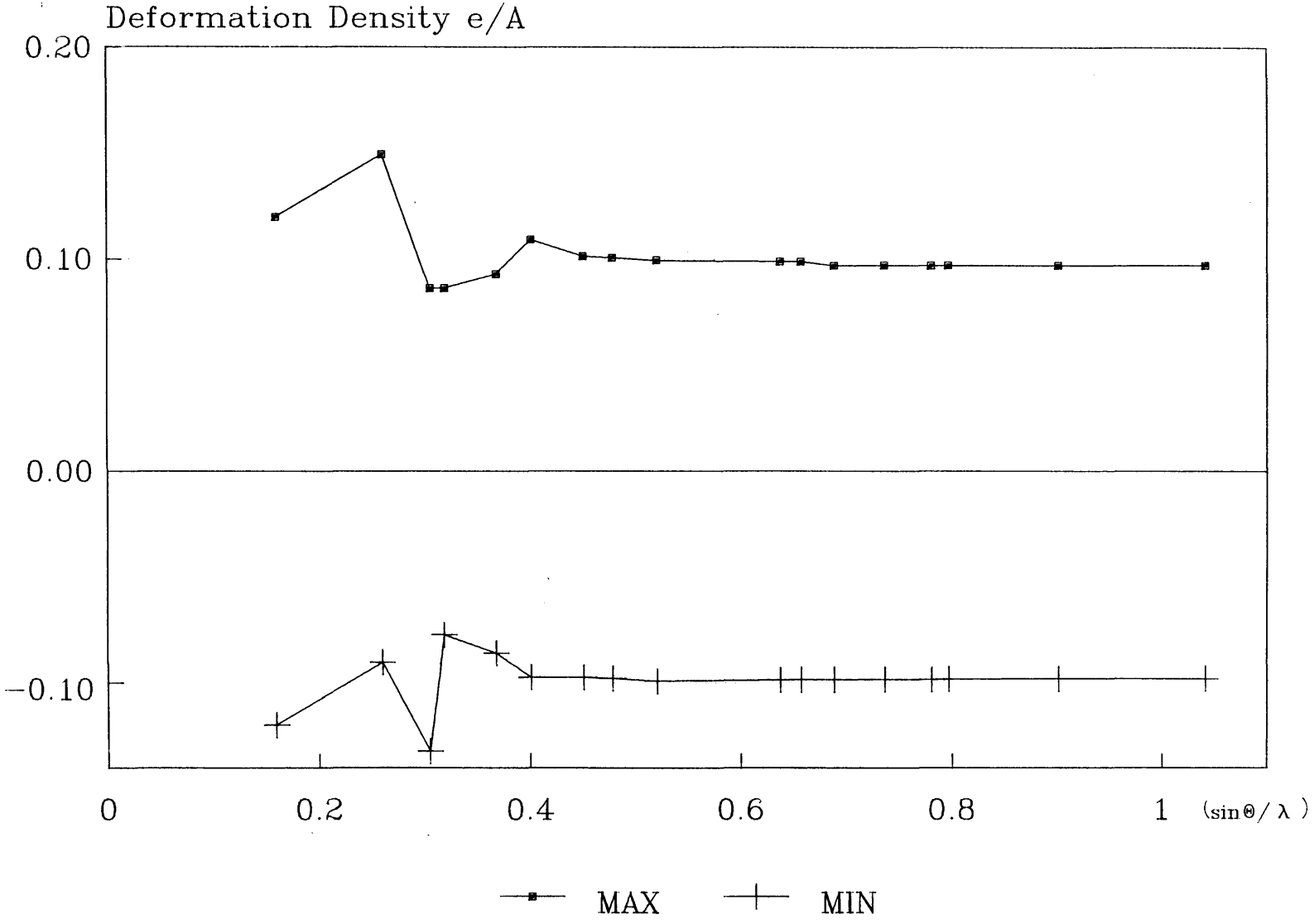
Deformation Density e/A
0.20
0.10
0.00
-0.10
0
0.2
0.4
0.6
0.8
1
(sinΘ/λ)
MAX
MIN

FIG.4

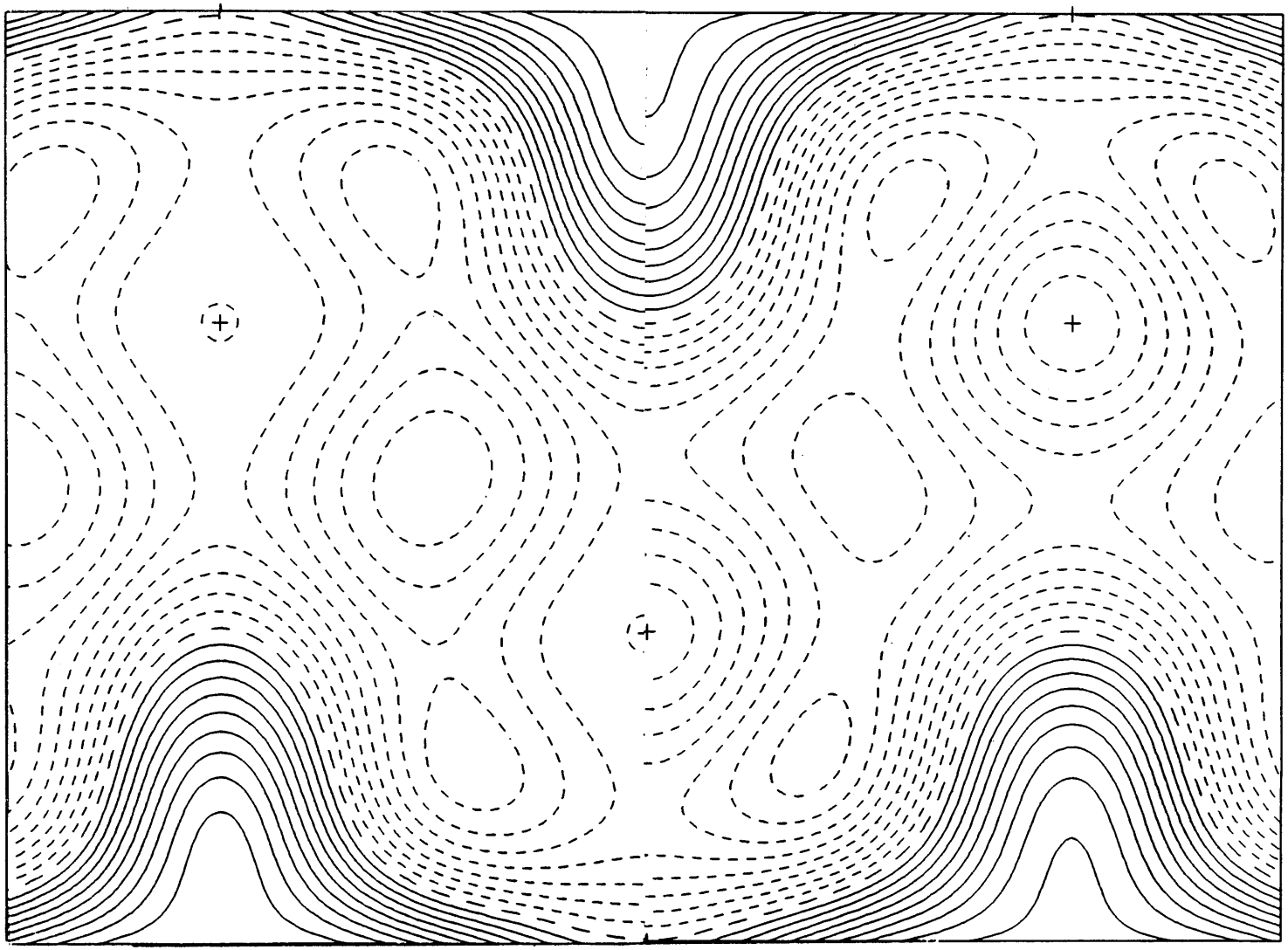

Fig. 5